Evaluation of liquefaction countermeasure effects on the performance of structures

Fernando Lopez-caballero, Esteban Saez, Arézou Modaressi-Farahmand-Razavi

Evaluation of liquefaction countermeasure effects on the performance of structures

Fernando Lopez-Caballero & Esteban Saez & Arezou Modaressi-Farahmand-Razavi
Laboratoire MSS-Mat CNRS UMR 8579, Ecole Centrale Paris, France

ABSTRACT: The present paper deals with the influence of soil non-linearity, introduced by soil liquefaction, on the soil-foundation-structure interaction phenomena. Numerical simulations are carried out so as to study an improvement method to reduce the liquefaction potential in a sandy soil profile subjected to a shaking. The efficiency of the confinement walls in the mitigation of a liquefiable soil is showed. However, the intervention at the foundation soil modifies the dynamic characteristics of soil-structure system and it seems to be an unfavorable method from the structural point of view.

1 INTRODUCTION

In practice, in order to mitigate the damaging effects of earthquake induced liquefaction in existing engineering structures, the countermeasure methods such as soil densification or diaphragm walls among others are used (Liu & Dobry 1995; Zheng et al. 1996; Adalier et al. 2003; Matsuda et al. 2005; Yasuda 2007). Such methods have been studied by several authors and the principal conclusion of these works is that the efficiency of each solution depends on many parameters (e.g. input signal characteristic, soil properties).

According to different results, other than the effects on the structure settlement, it seems that, in the case of large amplitude motion producing liquefaction phenomena in the soil foundation, the structural damage in structures with significant SSI effects may be reduced due to the local effects (Koutsourelakis et al. 2002; Ghosh & Madabhushi 2003; Popescu et al. 2006). Furthermore, for single-degree-of-freedom structures (SDOF) without soil structure interaction (SSI), their responses are principally in flexion mode, thus the SDOF can present great damage (i.e. damage due to the large induced drift) related to the liquefaction phenomena (Lopez-Caballero & Modaressi-Farahmand-Razavi 2008).

In the case where the mitigation method is efficient, it improves the properties of the soil producing a soil stiffening effect and the liquefaction risk is eliminated. However, the damping behaviour and the frequency content modification on the surface ground motion due to liquefaction apparition are reduced and consequently the structural drift could be increased.

The aim of this work is to use numerical methods in order to evaluate the efficiency of the confinement or diaphragm walls in the mitigation of liquefiable loose, saturated sand to a shaking and to estimate their effects on the earthquake motion transferred to the structure through the foundation. A 2D coupled finite element modelling is carried out. The ECP's elastoplastic multi-mechanism model, commonly called Hujeux model (Aubry et al. 1982; Hujeux 1985) is used to represent the soil behavior in the numerical Gefdyn code (Aubry et al. 1986; Aubry & Modaressi 1996). A SDOF structure founded on a rigid shallow foundation is chosen to reveal, with great simplicity, the beneficial or unfavorable effects of the proposed mitigation method.

2 NUMERICAL MODEL

The studied site is composed principally of overconsolidated clay layers overlaid by 29m of loose sand (i.e. a relative density $D_r < 50\%$). According to the test results and the soil description (Lopez-Caballero & Modaressi-Farahmand-Razavi 2008), it is deduced that the liquefaction phenomena can appear at layers between 4m and 15m depth. Thus, an elastoplastic model is only used to represent the soil behaviour on the top 29m. Figure 1 shows the finite element mesh of the numerical model for the parametric study.

So as to take into account the interaction effects between the structure and the plane-strain domain, a modified "*width plane strain*" condition (Saez 2008) was assumed in the finite element models. In this case a width of 4m is used.

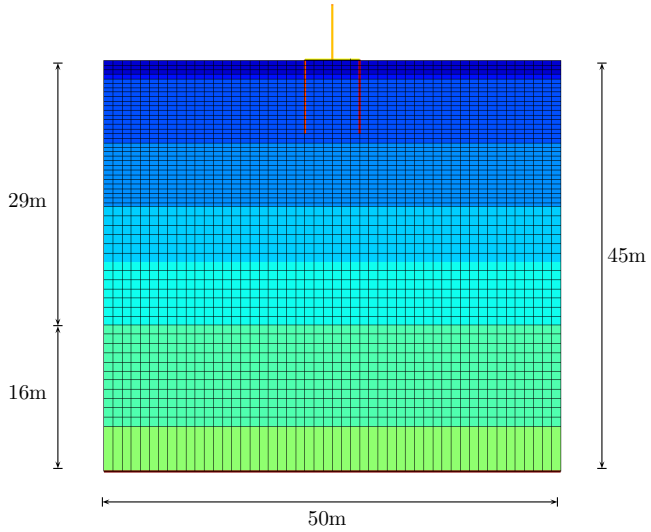

Figure 1. Used finite element mesh in the numerical model.

2.1 *Soil constitutive model*

The ECP's elastoplastic multi-mechanism model (Aubry et al. 1982; Hujeux 1985), commonly called Hujeux model is used to represent the soil behaviour. This model can take into account the soil behaviour in a large range of deformations. The model is written in terms of effective stress. The representation of all irreversible phenomena is made by four coupled elementary plastic mechanisms: three plane-strain deviatoric plastic deformation mechanisms in three orthogonal planes and an isotropic one. The model uses a Coulomb type failure criterion and the critical state concept. The evolution of hardening is based on the plastic strain (deviatoric and volumetric strain for the deviatoric mechanisms and volumetric strain for the isotropic one). To take into account the cyclic behaviour a kinematical hardening based on the state variables at the last load reversal is used. The soil behaviour is decomposed into pseudo-elastic, hysteretic and mobilized domains.

The model's parameters of the soil are obtained using the methodology suggested by Lopez-Caballero et al. (2007). In order to verify the model's parameters, the behaviour of the sand must be studied by simulating drained (DCS) and undrained cyclic shear tests (UCS). Figure 2 shows the responses of these DCS tests obtained by the model of the loose sand at $\sigma'_{mo} = 40$ and $80kPa$. The tests results are compared with the reference curves proposed by Seed et al. (1986).

The obtained curve of cyclic stress ratio (τ/σ'_m) as a function of the number of loading cycles to produce liquefaction (N) at $\sigma'_m = 40kPa$ is given in Figure 3. The modelled test result is compared with the reference curves given by Seed & Idriss (1982) for sands at different densities (i.e. SPT values). We can notice that the obtained curve matches relatively good with

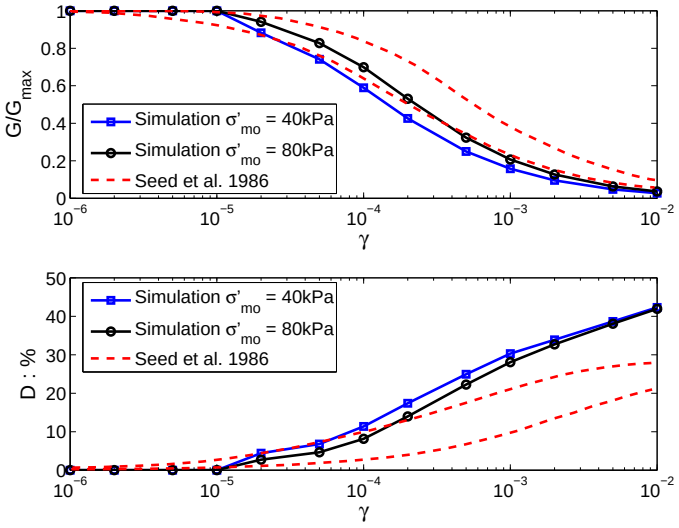

Figure 2. Comparison between simulated and reference curves obtained by Seed et al. (1986).

the one corresponding to $SPT - N_{60} = 5$.

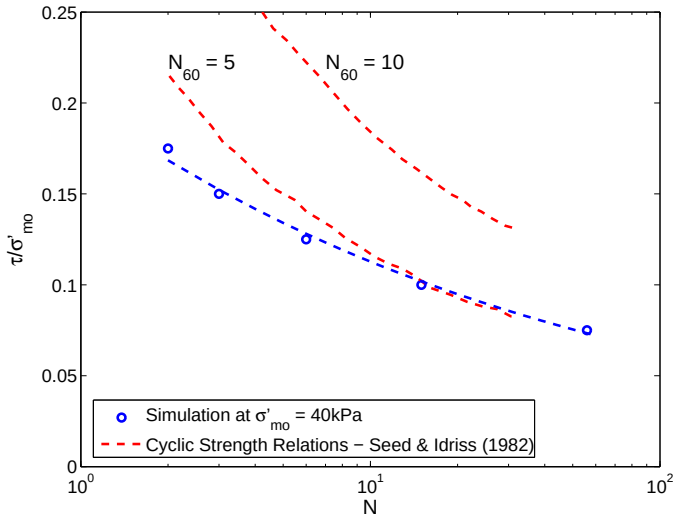

Figure 3. Comparison of simulated sand model liquefaction curves with cyclic strength relations.

2.2 *Structural model*

In order to simulate the single-degree-of-freedom (SDOF) structure a continuous isotropic elastic-plastic beam element is used. Non-linear structural behaviour is taken into account through an elastic-perfectly-plastic strain-stress relation. The characteristics of the SDOF structure used in this study are: elastic modulus, $E = 25.5GPa$; yielding stress of structural elements, $\sigma_y = 6.0MPa$; mass, $M = 20000kg$ and height, $h = 6.0$m. With this characteristics the SDOF fundamental period (T_{str}) is equal to 0.4s. Concerning the seismic demand evaluation, Figure 4 shows the corresponding capacity curve obtained modelling a pushover test. This curve is plotted using the maximum top displacement D and its corresponding base shear, in terms of spectral accel-

eration A. According to Hazus proposition (HAZUS-MH MR3 2003), the ultimate acceleration value corresponds approximately to moderate-code C1L.

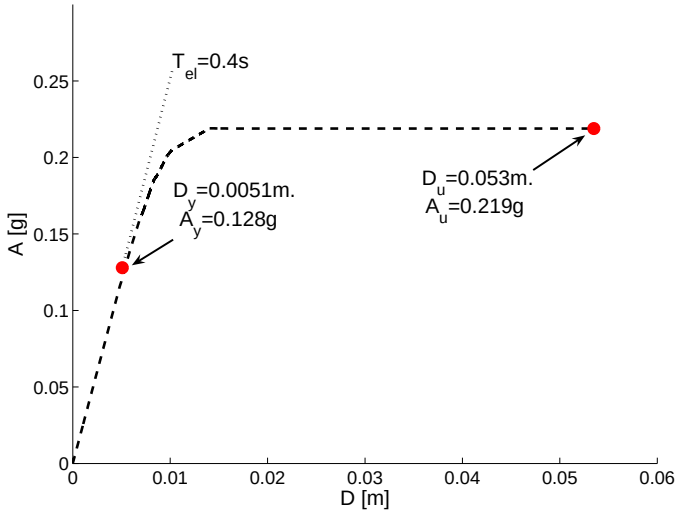

Figure 4. Obtained SDOF Capacity Curve. Fixed base test.

As regards the confinement walls, they are composed of 2 inclusions with 8m depth and a thicknesses of 0.5m. The distance between them is 6m and it is supposed that they are clamped to the foundation. The inclusions are simulated with continuous isotropic elastic beam elements with a Young modulus $E_{inc} = 25.5GPa$ (Fig. 5). They are supposed to be impervious. The interface between the liquefiable soil and the confinement wall was modelled using "*zero thickness*" interface elements with a rigid-plastic Mohr-Coulomb type model. The friction angle of the interface is assumed to be $23°$.

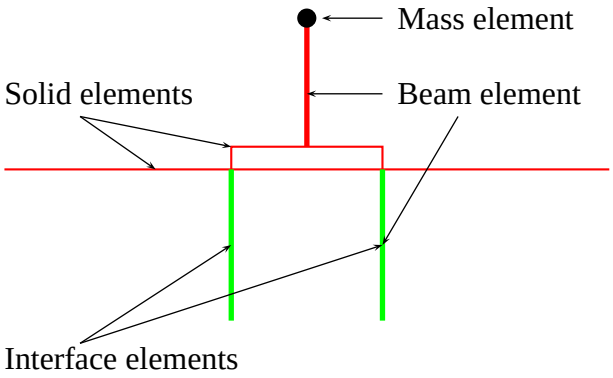

Figure 5. Illustration of remediation method used in the numerical model.

2.3 *Input earthquake motion*

The used seismic input motions are the acceleration time histories generated by a non-stationary stochastic simulation. The model is adapted from Pousse et al. (2006). The method depends on four common indicators in earthquake engineering: peak ground acceleration, strong-motion duration, Arias intensity (Arias 1970), and central frequency. These indicators are empirically connected to a given database by means of ground-motion prediction equations. In our case, the European prediction equations have been used. In this work, 20 synthetic earthquakes have been generated with a magnitude $M_s = 7.0$ and a distance of the source $D = 50$km. The generated motions will be used as outcropping input motion with amplitudes values from 0.05g to 0.20g. All signals are consistent with the response spectra of Type A soil of Eurocode8 (Fig. 6).

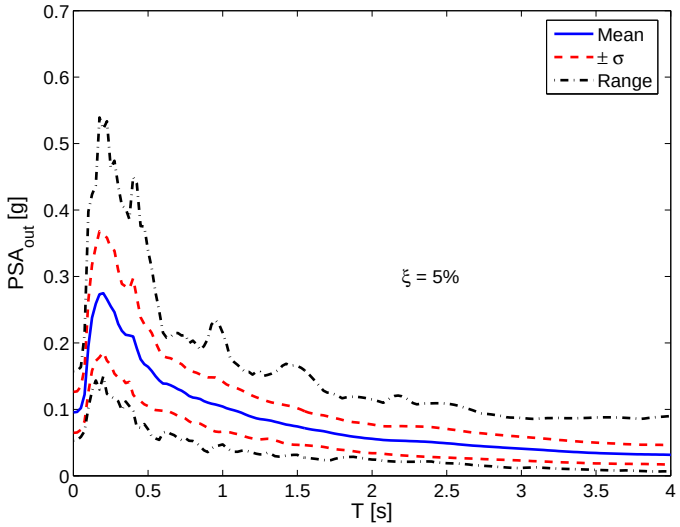

Figure 6. Response spectra of input earthquake motions.

2.4 *Boundary conditions*

In the analysis, only vertically incident shear waves are introduced into the domain and as the lateral limits of the problem are considered to be far enough, their response is assumed to be the response of a free field. Thus, equivalent boundaries have been imposed on the nodes of these boundaries (i.e. the normal stress on these boundaries remains constant and the displacements of nodes at the same depth in two opposite lateral boundaries are the same in all directions).

For the bedrock's boundary condition, paraxial elements simulating a "*deformable unbounded elastic bedrock*" have been used (Modaressi & Benzenati 1994). The incident waves, defined at the outcropping bedrock are introduced into the base of the model after deconvolution. Thus, the obtained movement at the bedrock is composed of the incident waves and the reflected signal. The bedrock is supposed to be impervious and the water level is placed at the ground surface.

3 LIQUEFACTION ANALYSIS

In order to define the liquefaction reference case, the responses obtained by the model without inclusions are analysed. Figure 7 shows the variation of peak ground acceleration (PGA) at the surface (FF) near to the structure (i.e. 12m far) and at the structure base as a function of the maximum acceleration at outcropping ($a_{max\ out}$). According to this figure, the amplification of peak ground acceleration on the ground surface relative to bedrock appears before $a_{max\ out}$ value equal to 0.12g. After this value, the non linear behaviour of soil profile, due principally to the apparition of liquefaction phenomenon, produces an attenuation of the seismic motion observed at the ground surface.

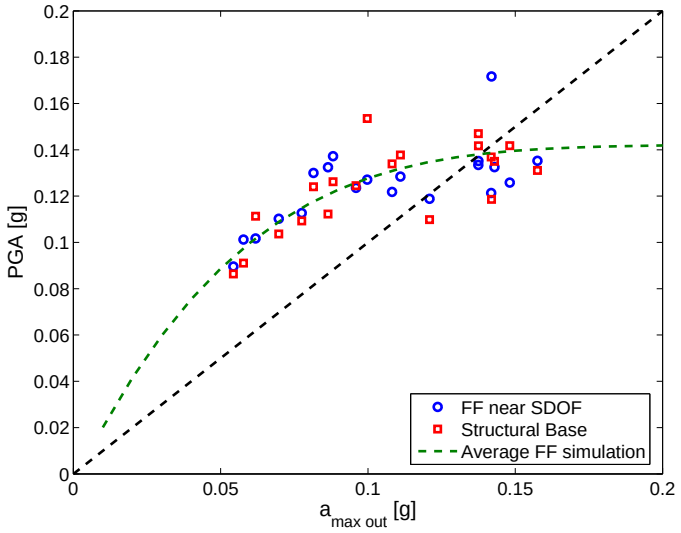

Figure 7. Relationships between maximum accelerations on bedrock and surface obtained in the soil profile.

It can be noted from the obtained pore pressure excess (Δp_w) in the soil profile below the foundation of SDOF (Fig. 8), that the liquefaction zone during the 20 earthquakes is placed at layers between 2 and 8m depth.

So as to quantify the effect of the liquefaction phenomena, we use the computed Liquefaction Index (Q) for the profile below the foundation. This parameter is defined by Shinozuka & Ohtomo (1989) as:

$$Q = \frac{1}{H}\int_0^H \frac{\Delta p_w(t,z)}{\sigma'_{vo}(z)}\,dz \qquad (1)$$

where H is the selected depth (in this case, $H = 16$m), $\Delta p_w(t,z)$ is the pore water pressure build-up computed at time t and depth z and $\sigma'_{vo}(z)$ is the initial effective vertical stress at depth z. Figure 9 provides the variation of Q value at the end of shaking with the the Arias intensity at outcropping ($I_{Arias\ out}$). In this study, the end of shaking is defined as the time t that corresponds to the 95% of Arias intensity $t_{95\%I_{Arias}}$.

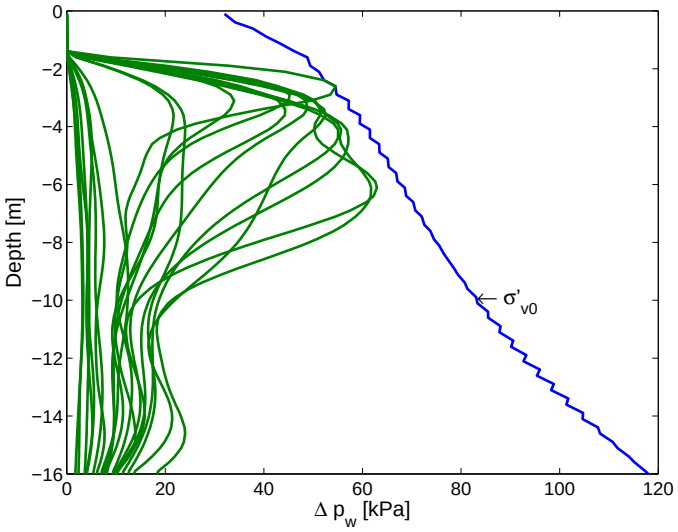

Figure 8. Obtained pore pressure excess in the soil profile below the foundation; evolution of maximum value with depth.

Referring again to Figure 9, it can be seen that as expected, the Q value increases with an increase in $I_{Arias\ out}$ value. It appears that $I_{Arias\ out}$ value provides a good correlation with the thickness of the zones where liquefaction takes place (i.e. the liquefaction index).

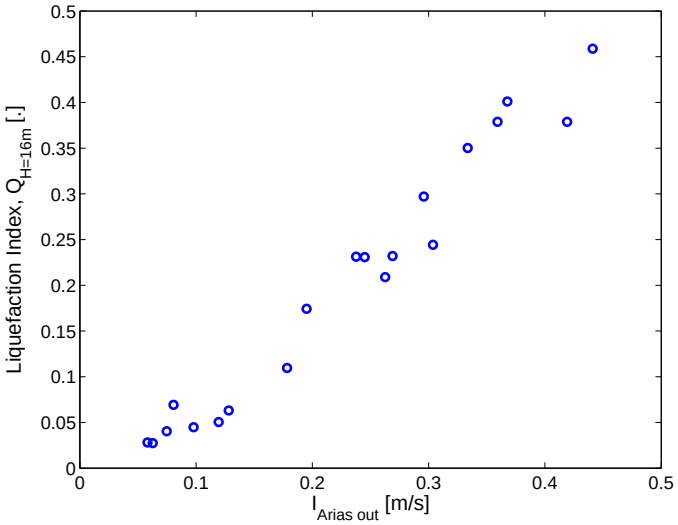

Figure 9. Obtained Liquefaction Index (Q) below the foundation as a function of $I_{Arias\ out}$ in non linear analyses for all cases.

As far as it concerns the relative co-seismic settlement induced by the liquefaction and according to Figure 10, it can be noted that, the higher Q value the higher induced settlement. According to Yasuda (2007), the large settlement induced is produced principally by the horizontal movement of the ground under the structure.

Regarding the response of soil structure system, according to the transfer function at FF (i.e. ratio of the frequency response at the soil surface over

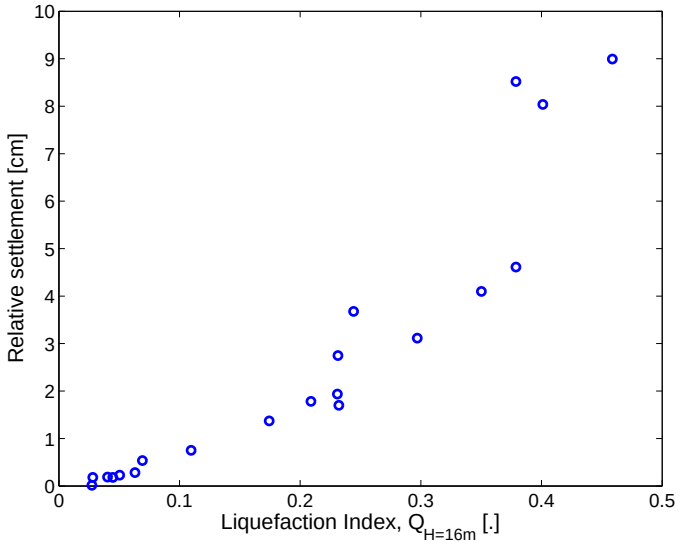

Figure 10. Variation of obtained relative settlement as a function of Liquefaction Index (Q) below the foundation.

the bedrock frequency response), the first natural frequency of the soil profile f_{soil} is found to be, for the linear elastic case, at $1.75Hz$ (i.e. $T_{soil} = 0.57$s). As expected, the SDOF ($f_{str} = 2.5Hz$), being more rigid than the soil (i.e. $f_{soil} < f_{str}$), presents an important interaction with the soil foundation.

Finally, with regard to seismic demand evaluation on the SDOF, the maximum top displacement D and its corresponding spectral acceleration A observed during the ISS computation are presented in Figure 11. In this figure, the corresponding capacity curve obtained by modelling the pushover test is also plotted. According to this figure, it is noted that a structural non-linear behaviour appears (i.e. $D > D_y$, where D_y is the displacement corresponding to the yield capacity of structure). If μ is defined as the ductility ratio ($\mu = D/D_y$, with $D_y = 0.51$cm from pushover test), in our cases the ductility ratio varies from 1.8 to 4.8.

4 ANALYSIS OF LIQUEFACTION IMPROVEMENT METHODS

In this section, a mitigation method (i.e. confinement walls) is used in order to improve the ground under the SDOF structure to prevent liquefaction. The selected mitigation method reduces the liquefaction potential stiffening the soil and decreases the settlement reducing the horizontal movement of soil.

The distribution of computed normalized pore pressure ratio ($R_u = \Delta p_w/\sigma'_{zo}$) below the foundation at the end of shaking for one case with and without inclusions are shown in Figure 12. A comparison of distribution of R_u into two profiles indicates that, below the foundation the level of R_u decreases strongly when the inclusions are used. However, outside of the inclusions area, i.e. at the free field, the R_u values are

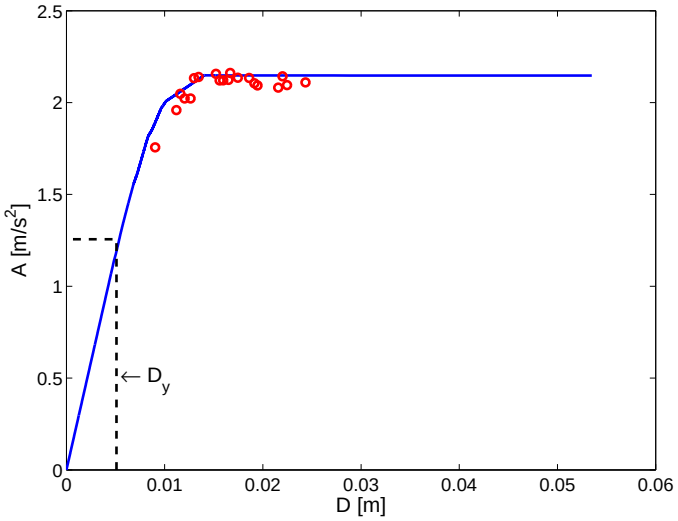

Figure 11. Structural dynamic response obtained for the SDOF compared with the static capacity curve.

near to 1.0 in both cases and the liquefaction phenomena appears.

Now, comparing the induced maximum shear strain at different depths of the profile below the foundation for the same input signal (Fig. 13), it is interesting to note that near the surface level, the cyclic shear strain values decrease when the inclusions are used. On the other hand, an opposite behaviour is observed in the soil below the inclusions. Thus, it confirms that the mitigation efficiency is due to the soil stiffening effect.

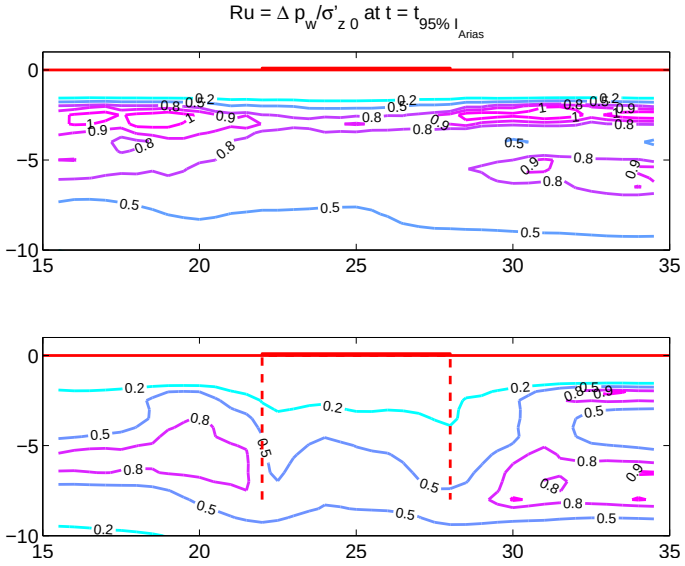

Figure 12. Comparison of the distribution of excess pore pressure ratio ($R_u = \Delta p_w/\sigma'_{zo}$), for one case with (below) and without (above) inclusions.

In order to quantify the mitigation efficiency of the different configurations, the computed Liquefaction Index (Q) below the foundation for the profile with and without inclusions are compared (Fig. 14). It can be seen that the Q values decrease when the soil is improved. However, it is noted that in some cases,

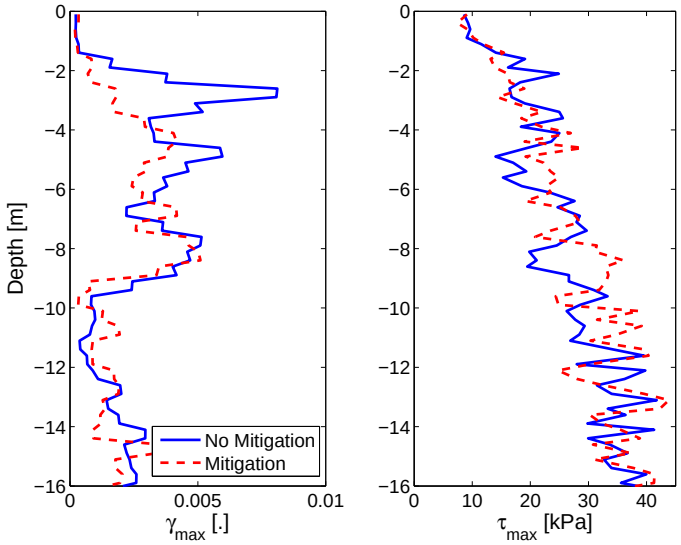

Figure 13. Induced maximum shear strain γ_{max} and maximum shear stress τ_{max} on the soil profile for one case with and without inclusions.

the value of Q obtained after soil mitigation is greater than the reference case.

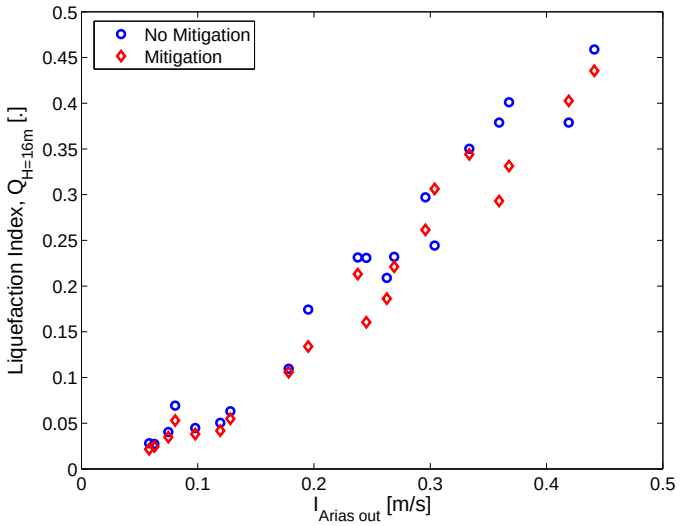

Figure 14. Comparison of Liquefaction Index (Q) obtained below the foundation as a function of $I_{Arias\ out}$ for the profile with and without inclusions.

Figure 15 provides a comparison of pore pressure excess Δp_w profile in two cases, when the mitigation is efficient and when it is not. In the second case, even if the inclusion reduces the Δp_w at the soil surface level (i.e. above 4m) in relation to the reference case, it produces a pore pressure build up between 5 and 7m depth (Fig. 15). It means that the mitigation efficiency is a function of the inclusion stiffness and the soil around it.

As already mentioned, the remediation method used increases the liquefaction strength and decreases the settlement of the structure. As illustrated in Figure 16, the co-seismic structural settlement obtained after soil improvement is greatly reduced as a consequence

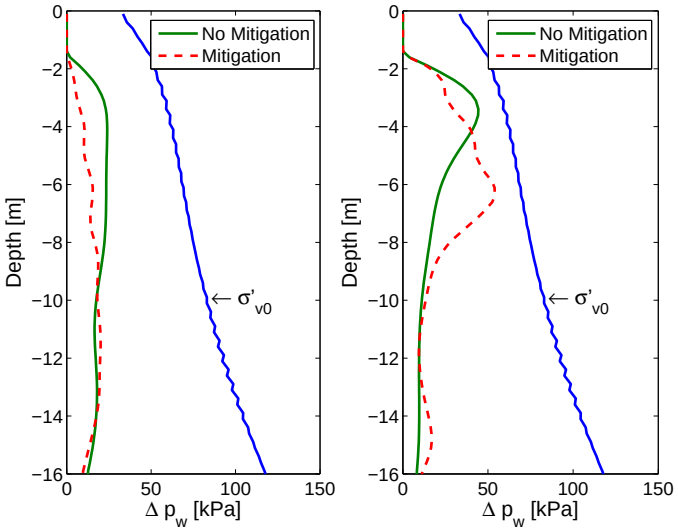

Figure 15. Comparison of pore pressure excess in the soil profile obtained below the foundation for the profile with and without inclusions.

of soil stiffening.

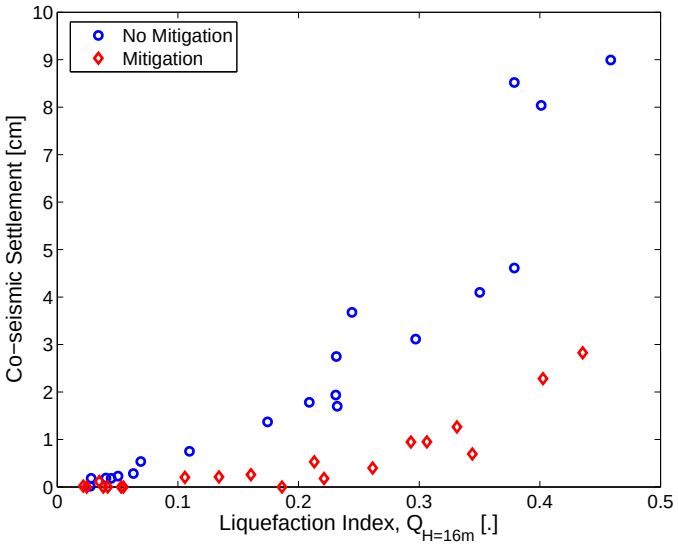

Figure 16. Scatter plot of relative settlement as a function of Liquefaction Index (Q) below the foundation with and without mitigation.

The beneficial or unfavorable effects of the mitigation methods on the structural behaviour could be illustrated comparing the responses obtained for the profile with and without inclusions using relative ratios such as: $\Delta Q = (Q_{mit} - Q_o)/Q_o$ for the liquefaction potential and $\Delta\mu = (\mu_{mit} - \mu_o)/\mu_o$ for structural behaviour. Where mit and o subscripts refer to values after and before mitigation respectively.

In order to evaluate the effect of the introduction of the improvement methods of liquefaction on the behaviour of the superstructure, the scatter plot of Figure 17 is provided. It should be noted that, concerning the increase of pore water pressure, it is reduced by the presence of the inclusions (i.e. $\Delta Q \leq 0$, zones II and III), thus it is a beneficial method concerning the

liquefaction phenomena. However, regarding the variation of ductility ratio μ of the structure, it appears that in some cases, it increases because of the soil stiffening effect (i.e. $\Delta\mu \geq 0$, zones I and II), hence it is an unfavorable method from the structural point of view. Thus, judging from these results, in addition to soil improvement it is also necessary to strengthen the structure in order to prevent its higher damage.

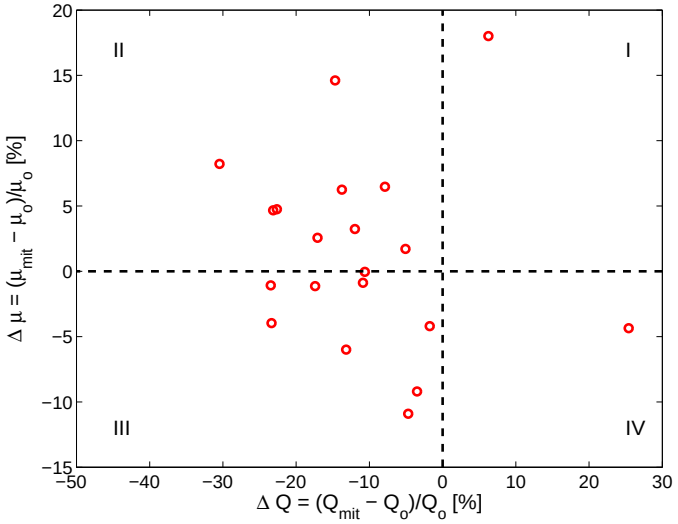

Figure 17. Scatter plot of variation of ductility ratio $\Delta\mu$ with respect to variation of liquefaction index ΔQ.

5 CONCLUSIONS

A series of finite element parametric analyses were used to investigate the effects of the liquefaction countermeasure methods on the behaviour of existing structures. A typical soil-structure model has been used to illustrate key results from parametric studies. The main conclusions drawn from this study are as follows:

1. According to the responses obtained with the model without mitigation, it can be concluded that the choice of the "*bedrock*" signal remains the most subtle parameter in order to define the liquefiable zones and the characteristics of possible countermeasure methods. Thus, a parametric analysis is needed in order to study the influence of several signal parameters on the response of the site soil profile.

2. The analyses showed that the use of the vertical inclusions reduces the excess pore pressure ratio underneath the structure. The mitigation efficiency is due to the soil stiffening effect allowing to reduce the structural settlement.

3. As far as it concerns the effect of soil improvement on the structural behaviour, it appears that in some cases, the ductility ratio increases by the soil stiffening effect, hence it is an unfavorable method from the structural point of view. As a result, it is necessary to strengthen the structure in order to prevent its collapse.

ACKNOWLEDGEMENTS

This study has been done in the framework of both the European Community Contract No GRDI-40457, NEMISREF (*New methods of mitigation of seismic risk on existing foundations*) and the French project ANR-06-CATT-003-01, BELLE-PLAINE.

REFERENCES

Adalier, K., Elgamal A.-W., Meneses J., & Baez J. I. 2003. Stone columns as liquefaction countermeasure in non-plastic silty soils. *Soil Dynamics and Earthquake Engineering 23*(7), 571–584.

Arias, A. 1970. A mesure of earthquake intensity. In *Seismic Design for Nuclear Power Plants*, pp. 438–483. R.J. Hansen (ed.), MIT Press, Cambridge, Massachusetts.

Aubry, D., Chouvet D., Modaressi A., & Modaressi H. 1986. GEFDYN: Logiciel d'Analyse de Comportement Mécanique des Sols par Eléments Finis avec Prise en Compte du Couplage Sol-Eau-Air. Manuel scientifique, Ecole Centrale Paris, LMSS-Mat.

Aubry, D., Hujeux J.-C.,Lassoudière F., & Meimon Y. 1982. A double memory model with multiple mechanisms for cyclic soil behaviour. In *Int. Symp. Num. Mod. Geomech*, pp. 3–13. Balkema.

Aubry, D. & Modaressi A. 1996. GEFDYN. Manuel scientifique, Ecole Centrale Paris, LMSS-Mat.

Ghosh, B. & Madabhushi S. P. G. 2003. Effects of localised soil inhomogenity in modyfyng seismic soil structure interaction. In *16th ASCE Engineering Mechanics Conference*. University of Washington, Seattle.

Hujeux, J.-C. 1985. Une loi de comportement pour le chargement cyclique des sols. In *Génie Parasismique*, pp. 278–302. V. Davidovici, Presses ENPC, France.

Koutsourelakis, S., Prévost J. H., & Deodatis G. 2002. Risk assessment of an interacting structure-soil system due to liquefaction. *Earthquake Engineering and Structural Dynamics 31*(4), 851–879.

Liu, L. & Dobry R. 1995. Effect of liquefaction on lateral response of piles by centrifuge model tests. *National Center for Earthquake Engineering Research (*NCEER*) Bulletin 9*(1), 7–11.

Lopez-Caballero, F. & Modaressi-Farahmand-Razavi A. 2008. Numerical simulation of liquefaction effects on seismic SSI. *Soil Dynamics and Earthquake Engineering 28*(2), 85–98.

Lopez-Caballero, F., Modaressi-Farahmand-Razavi A., & Modaressi H. 2007. Nonlinear numerical method for earthquake site response analysis i- elastoplastic cyclic model & parameter identification strategy. *Bulletin of Earthquake Engineering 5*(3), 303–323.

Matsuda, T., Tanaka K., & Okano M. 2005. Advanced in-service seismic retrofitting methods for a railway viaduct. In *Proccedings 1st Greece-Japan Workshop : Seismic design, observation and retrofit of foundations*, A*thens*, pp. 277–287. Gazetas et al. Eds.

Modaressi, H. & Benzenati I. 1994. Paraxial approximation for poroelastic media. *Soil Dynamics and Earthquake Engineering 13*(2), 117–129.

Popescu, R., Prévost J. H., Deodatis G., & Chakrabortty P. 2006. Dynamics of nonlinear porous media with applications to soil liquefaction. *Soil Dynamics and Earthquake Engineering 26*(6-7), 648–665.

Pousse, G., Bonilla F., Cotton F., & Margerin L. 2006. Non stationary stochastic simulation of strong ground motion time histories including natural variability: Application to the K-net Japanese database. *Bulletin of the Seismological Society of America 96*(6), 2103–2117.

Saez, E. 2008. *Dynamic non-linear Soil-Structure Interaction*. PhD thesis, École Centrale Paris, France.

Seed, H. B. & Idriss I. M. 1982. Ground motion and soil liquefaction during earthquakes. Monograph series, earthquake engineering research institute, University of California, Berkeley, CA.

Seed, H. B., Wong R. T., Idriss I. M., & Tokimatsu K. 1986. Moduli and damping factors for dynamic analyses of cohesionless soils. *Journal of Geotechnical Engineering - ASCE 112*(11), 1016–1032.

Shinozuka, M. & Ohtomo K. 1989. Spatial severity of liquefaction. In *Proceedings of the second US-Japan workshop in liquefaction, Large Ground Deformation and Their Effects on Lifelines*.

HAZUS-MH MR3 2003. Multi-hazard Loss Estimation Methodology. Technical Manual. Report FEMA, Federal Emergency Management Agency.

Yasuda, S. 2007. Remediation methods againts liquefaction which can be applied to existing structures. In *Earthquake Geotechnical Engineering*, pp. 385–406. K.D. Pitilakis Ed., Springer, The Netherlands.

Zheng, J., Suzuki K., Ohbo N., & Prevost J.-H. 1996. Evaluation of sheet pile-ring countermeasure against liquefaction for oil tank site. *Soil Dynamics and Earthquake Engineering 15*(6), 369–379.